

Original Research

Pyroptosis-Related Subtypes Predict the Response of Clear Cell Renal Cell Carcinoma to Targeted Therapy

Jinpeng Ma^{1,2,†}, Zhijian Kang^{1,2,†}, Guang Yang^{3,†}, Xinyue Wang^{1,2}, Mingguai Si^{1,2}, Yuting Wang^{1,2}, Guangbin Li^{1,2}, Shiyu Bai^{1,2}, Fanshu Zeng^{1,2}, Min Li^{1,2}, Ziqi Wang^{1,4,*}, Lu Wang^{1,2,*}, Wanhai Xu^{1,4,*}

¹NHC Key Laboratory of Molecular Probes and Targeted Diagnosis and Therapy, Harbin Medical University, 150001 Harbin, Heilongjiang, China

²Department of Urology, The Fourth Hospital of Harbin Medical University, Heilongjiang Key Laboratory of Scientific Research in Urology, 150081 Harbin, Heilongjiang, China

³Department of Neurosurgery, The First Affiliated Hospital of Harbin Medical University, 150001 Harbin, Heilongjiang, China

⁴Department of Urology, Harbin Medical University Cancer Hospital, 150001 Harbin, Heilongjiang, China

*Correspondence: wangziqi@hrbmu.edu.cn (Ziqi Wang); wanglu@hrbmu.edu.cn (Lu Wang); xuwanhai@hrbmu.edu.cn (Wanhai Xu)

†These authors contributed equally.

Academic Editor: Viviana di Giacomo

Submitted: 20 March 2023 Revised: 30 June 2023 Accepted: 11 August 2023 Published: 8 December 2023

Abstract

Background: Pyroptosis plays a crucial role in anti-tumor immunity and in formation of the immune microenvironment. However, whether pyroptosis is involved in the progression of clear cell renal cell carcinoma (ccRCC) is still unclear. Personalized treatment of ccRCC requires detailed molecular classification to inform a specific therapy. **Methods:** Molecular subtyping of ccRCC was performed based on consensus clustering of pyroptosis-related genes. The characteristics of these molecular subtypes were explored at the genome, transcriptome and protein levels. Single-cell RNA sequencing and CIBERSORT analysis were used to analyse the immune microenvironment of ccRCC, while Lasso regression was used to develop a prediction model based on hub genes. Expression of the pyroptosis-related gene *GSDMB* was also investigated at the tissue and cellular levels. **Results:** Two molecular subtypes were identified based on the clustering of pyroptosis-related genes. Cluster 1 was associated with activation of classical oncogenic pathways, especially the angiogenesis pathway. Cluster 2 was associated with activation of immune-related pathways and high levels of immunosuppressive cells, exhausted CD8⁺ T cells, and tumor-associated fibroblast infiltration. Clusters 1 and 2 were thus defined as the angiogenic and inflamed subtypes, respectively. The two subtypes were predictive of the response of ccRCC to anti-angiogenic therapy and immunotherapy, with Cluster 1 patients benefiting from anti-angiogenic therapy and Cluster 2 patients showing better response to anti-PD1 inhibitor therapy. Furthermore, a 9-gene expression signature (*HJURP*, *NUF2*, *KIF15*, *MELK*, *TPX2*, *PLK1*, *CDCA3*, *CTLA4*, *FOXP3*) was identified that could predict outcome and response to immune checkpoint blockade therapy in test cohorts. Finally, *GSDMB* was found to be involved in the development of renal clear cell carcinoma. **Conclusions:** These results on pyroptosis-related genes in ccRCC provide a theoretical basis for understanding molecular heterogeneity and for the development of individualized treatment strategies.

Keywords: pyroptosis; immune microenvironment; immunotherapy; clear cell renal carcinoma

1. Introduction

Worldwide, approximately 431,000 patients are diagnosed annually with renal carcinoma (RCC), with about 179,000 deaths resulting from this disease [1]. RCC is one of the most common tumors of the urinary system [2]. The most common pathologic type of RCC is clear cell renal cell carcinoma (ccRCC), which accounts for 70–75% of cases [3,4]. Partial nephrectomy or radical nephrectomy is usually the first treatment choice for patients with early RCC, with a 5-year survival rate of 80–90% [5]. However, about 30% of RCC patients relapse within 5 years after surgery [6]. Clear cell renal cell carcinoma is not sensitive to chemoradiotherapy [3]. Immunotherapy and anti-angiogenic therapy, either as monotherapy or in combination, have significantly improved the clinical outcome of patients with advanced RCC. However, not all patients are

responsive to these therapies. ccRCC is an extremely heterogeneous tumor, and patients with the same pathological type can have different characteristics. Therefore, it is critical to understand the molecular basis for the clinical heterogeneity observed in ccRCC patients. This will allow for more informed treatment selection and a deeper understanding of the resistance mechanisms [7].

Pyroptosis is a caspase-dependent, inflammatory cell death type characterized by pore-formation, cell swelling, disruption of the plasma membrane, and the release of cellular contents. A major trigger for pyroptosis is the gasdermin family (gasdermin A, B, C, D, E and pejkakin). Pyroptosis is primarily induced by multiple inflammasomes and is carried out by caspases and gasdermin proteins, leading to the formation of membrane pores and the secretion of cellular contents. Pyroptosis may have differ-



ent effects in tumors depending on the tissue origin and the tumor background. On one hand, pyroptosis can suppress cancer development. Independently of caspases, cytotoxic lymphocytes can induce pyroptosis in tumor cells that expressing GSDMB. NLRP3 expression is negatively correlated with hepatocellular carcinoma grade and stage. Additionally, NLRP1 has been associated with the stage and prognosis of colorectal cancer [8]. A low level of GSDME expression is associated with increased resistance to paclitaxel. Moreover, inflammatory cellular content is released following pyroptosis and membrane perforation, thus promoting cancer progression in various ways [9]. Elevated GSDMD expression is associated with tumor-node-metastasis and larger tumor size in non-small cell lung cancer [10]. Furthermore, high GSDMB expression is associated with poor prognosis and metastasis in breast cancer. These results indicate that pyroptosis-related genes can play dual roles in tumor progression. However, the roles and mechanisms of pyroptosis-related genes in ccRCC are still unclear. The purpose of this study was to illustrate whether pyroptosis could serve as a basis for individualized treatment of ccRCC patients.

2. Materials and Methods

2.1 Data Sources

Gene expression data (transcripts per million, TPM) and the relevant ccRCC prognostic and clinical data were obtained from The Cancer Genome Atlas (TCGA) (<https://portal.gdc.cancer.gov/>) databases. GSE40435, GSE53757, GSE121636, and GSE156632 were obtained from the Gene Expression Omnibus (GEO) (<https://www.ncbi.nlm.nih.gov/geo/>). RPPA protein expression data were obtained from ucsc xena (<https://xena.ucsc.edu/>). The E-MTAB-1980, E-MTAB-3267 and E-MTAB-3218 datasets were obtained from the ArrayExpress database (<https://www.ebi.ac.uk/arrayexpress/>). CheckMate 025 was obtained from (CM-025; NCT01668784) and CheckMate-010 from (CM-010; NCT01354431). The IMvigor210 cohort was downloaded from IMvigor210CoreBiologies. A schematic diagram of the study design is shown in **Supplementary Fig. 1**.

2.2 Consensus Clustering

Molecular subtypes based on pyroptosis-related genes were identified by the “ConsensusClusterPlus” package. Repetitions were performed 1000 times to ensure the stability of results [11].

2.3 Gene Set Variation Analysis (GSVA)

GSVA enrichment was performed using the “GSVA” R package [12]. The “limma” package was used to identify differentially expressed genes (DEGs) [13]. The selection of differentially expressed genes was an adjusted p -value less than 0.05 and an absolute value of \log_2 Fold Change ≥ 0.1 .

2.4 Cell Infiltration of the Tumor Microenvironment

Immune cells in the tumor microenvironment (TME) were quantified using the CIBERSORTx algorithm and MCP-counter [14,15]. Tumor purity scores were estimated with the “ESTIMATE” package [16]. The Tumor Immune Estimation Resource (TIMER) database was used to evaluate the TME [17] (**Supplementary Table 1**).

2.5 Cancer-Immune Cycle Analysis

The cancer immune cycle reflects the anticancer immune response and is comprised of 7 steps [18] (**Supplementary Table 2**). The relative activities of these steps determine the fate of tumor cells. The activity of each step was analyzed by single-sample gene set enrichment analysis (ssGSEA) based on gene expression of each samples [19].

2.6 Establishment of a Model for Prognostic Analysis

DEGs (\log_2 Fold Change > 0.5) were identified using a protein interaction algorithm and STRING analysis tool. Thirty central nodes with optimal connectivity were identified using the CytoHubba’s Maximal Click Centrality (MCC) function, and a prediction model was established using LASSO-Cox analysis [20]. Kaplan-Meier analysis was used to evaluate patient survival, and a time-dependent receiver operating characteristic (ROC) curve was used to evaluate the accuracy of the model.

2.7 Processing of Single-Cell RNA-seq Libraries and Batch Effect Correction

Barcodes with < 5000 total UMIs (Unique Molecular Identifiers), < 200 genes expressed, or mitochondrial genes were filtered out. Highly expressed genes were selected by genes that retained at least 3 UMIs in at least 200 cells [21]. Cells were separated by coarse clustering using the scatter v1.12.2 package [22]. Perform Principal Component Analysis (PCA) on normalized data and correct for batch effects on the top 200 PCs using the Mutual Nearest Neighbors (MNN) method [23].

2.8 Cell Lines and Cell Culture

The human normal cortex/proximal tubule epithelial cell line HK-2 and two renal clear cell carcinoma cell lines, 769-P and Caki-1, were from the Chinese Academy of Sciences Cell Bank (Shanghai, China). The HK-2, 769-P and Caki-1 cell lines were cultured in Dulbecco’s modified Eagle’s medium (biosharp, Hefei China), RPMI 1640 Medium (biosharp, China) and McCoy’s 5a Modified Medium (biosharp, China), respectively. This was added with 10% fetal bovine serum (VivaCell BIOSCIENCES, Hefei, China), 100 U/mL penicillin and 100 $\mu\text{g}/\text{mL}$ streptomycin (Gibco, New York, NY, USA). All cell lines were found to be mycoplasma-free using the MycAway™ Plus-Color One-Step Mycoplasma Detection Kit (Yeasen

Biotechnology, Shanghai, China) and were authenticated shortly before use with a PCR technique (Procell Corporation, Wuhan, China).

2.9 RNA Extraction and qRT-PCR

RNA was isolated from paracancerous and tumor tissues (16 pairs) using TRIZOL reagent (Invitrogen, Waltham, MA, USA) according to the manufacturer's protocol. Tumor tissues and paracancerous were collected from 16 ccRCC patients in the Department of Urology, Fourth Affiliated Hospital of Harbin Medical University. Informed consent was obtained and signed by patients for all tissues. The use of tissues was approved by the Ethics Committee of the Fourth Affiliated Hospital, Harbin Medical University. The ReverTraAce Qpcr RT Kit (Toyobo, Tokyo, Japan) was used for qRT-PCR experiments. The following primers were used for qRT-PCR: GSDMB: 5'-AGTCTTTGGGTTTCGGAGGAT-3' (F), 5'-CTGTCTGGGTCCTCCATGT-3' (R); ACTB: 5'-CTTCCTCCTGGGCATGG-3' (F), 5'-GCCGCCAGACAGCACTGT-3' (R).

2.10 Western Blot

The protein expression level in cell lines was determined by Western blot analysis. Protease inhibitors were used to isolate and lyse samples in RIPA buffer (Beyotime, Shanghai, China). Western blot was performed using rabbit polyclonal antibody against GSDMB (12885-1-AP, ProteinTech Group, Chicago, IL, USA) and mouse monoclonal antibody against β -actin (66009-1-Ig, ProteinTech Group, Chicago, IL, USA).

2.11 Tissue Samples and Immunohistochemistry (IHC)

A total of 35 tissue specimens were collected from 35 patients in the Department of Urology, Fourth Affiliated Hospital of Harbin Medical University. The use of tissues was approved by the Ethics Committee of the Fourth Affiliated Hospital, Harbin Medical University. GSDMB protein expression in low- and high-grade ccRCC and in normal tissues was assessed by IHC. Paraffin-embedded samples were deparaffinized, rehydrated, and placed in citrate buffer at 98 °C for 15 min for antigen retrieval. They were then incubated with anti-GSDMB antibody (Proteintech, 1:200 dilution). The expression was then examined by DAB kit (ORIGIN, Beijing, China).

2.12 Statistical Analysis

Correlation coefficients were calculated using Spearman analysis and distance correlation analysis. The log-rank test was used to determine the significance of differences between survival curves. ROC curves and the area under the curve (AUC) were obtained using the "pROC" and "timeROC" packages. Clinical characteristics were compared by chi-square or Fisher's exact test.

3. Results

3.1 Overview of Pyroptosis-Related Genes in ccRCC

Many clinical and genomic studies have shown that ccRCC is a high immune-infiltrating tumor type [24]. In the present study, the immune score for ccRCC was significantly correlated with poor overall survival (OS) and with tumor grade and stage (Fig. 1a, **Supplementary Fig. 2**), in accordance with the findings of a recent study [25]. Cytokines produced by pyroptotic cells recruit immune cells that subsequently infiltrate the TME, thereby having a tumor-promoting or suppressive role [26]. Pyroptosis therefor plays a significant role in the progression of ccRCC. The differential expression of pyroptosis-related genes (PRGs) between ccRCC and normal tissue is shown in **Supplementary Fig. 3**. Univariate cox analysis was used to identify genes associated with overall survival in ccRCC. Twelve genes (*AIM2*, *CASP4*, *GSDMB*, *GSDME*, *NLRP1*, *NLRP6*, *NOD2*, *NLRP1*, *NLRP6*, *PYCARD*, *SCAF11*, *TIRAP* and *HMGB1*) were selected for subsequent analyses due to having $p < 0.05$. However, only *NLRP6*, *SCAF11*, *TIRAP*, and *HMGB1* were potentially protective genes (i.e., hazard ratio (HR) < 1) for ccRCC patients, with the remaining genes being associated with increased risk (HR > 1) (Fig. 1b). A pyroptosis network was created to demonstrate the comprehensive landscape of PRG interactions, regulations and connections, together with their prognostic value in ccRCC patients (Fig. 1c). The expression of these PRGs (\log_2 FC > 1) in the TME, as determined by single-cell RNA sequencing, is presented in Fig. 1d–f and in **Supplementary Fig. 4**.

3.2 Cluster 1: Angiogenesis Phenotype

The molecular mechanisms underlying the heterogeneity of ccRCC were studied with the aim of optimizing personalized treatment strategies. Using unsupervised clustering, two different patterns were identified based on the expression profiles of PRGs with prognostic value (\log_2 Fold Change > 1). These were comprised of 330 samples in Cluster 1, and 196 samples in Cluster 2 (Fig. 2a, **Supplementary Fig. 5**). Survival analysis showed that patients in Cluster 2 had worse overall survival than patients of Cluster 1 ($p < 0.001$) (Fig. 2b). Biological functions were assessed by GSEA enrichment analysis between the two subtypes. Cluster 1 was associated with oncogenic pathways such as mTOR, Notch, MAPK, Wnt signalling, metabolic pathways, cell cycle, and DNA damage response. Cluster 2 contains more immune-related pathways, including antigen processing and presentation, and cytokine-cytokine receptor interactions, implying this subgroup may be involved in the tumor immunological process (Fig. 2d). Furthermore, Cluster 2 had higher immune and stromal scores compared with cluster 1, cluster 2 had higher immune and stromal scores Cluster 1 (Fig. 2c), implying the clusters had distinctive TME cell-infiltrating properties. Further investigation of the stromal composition re-

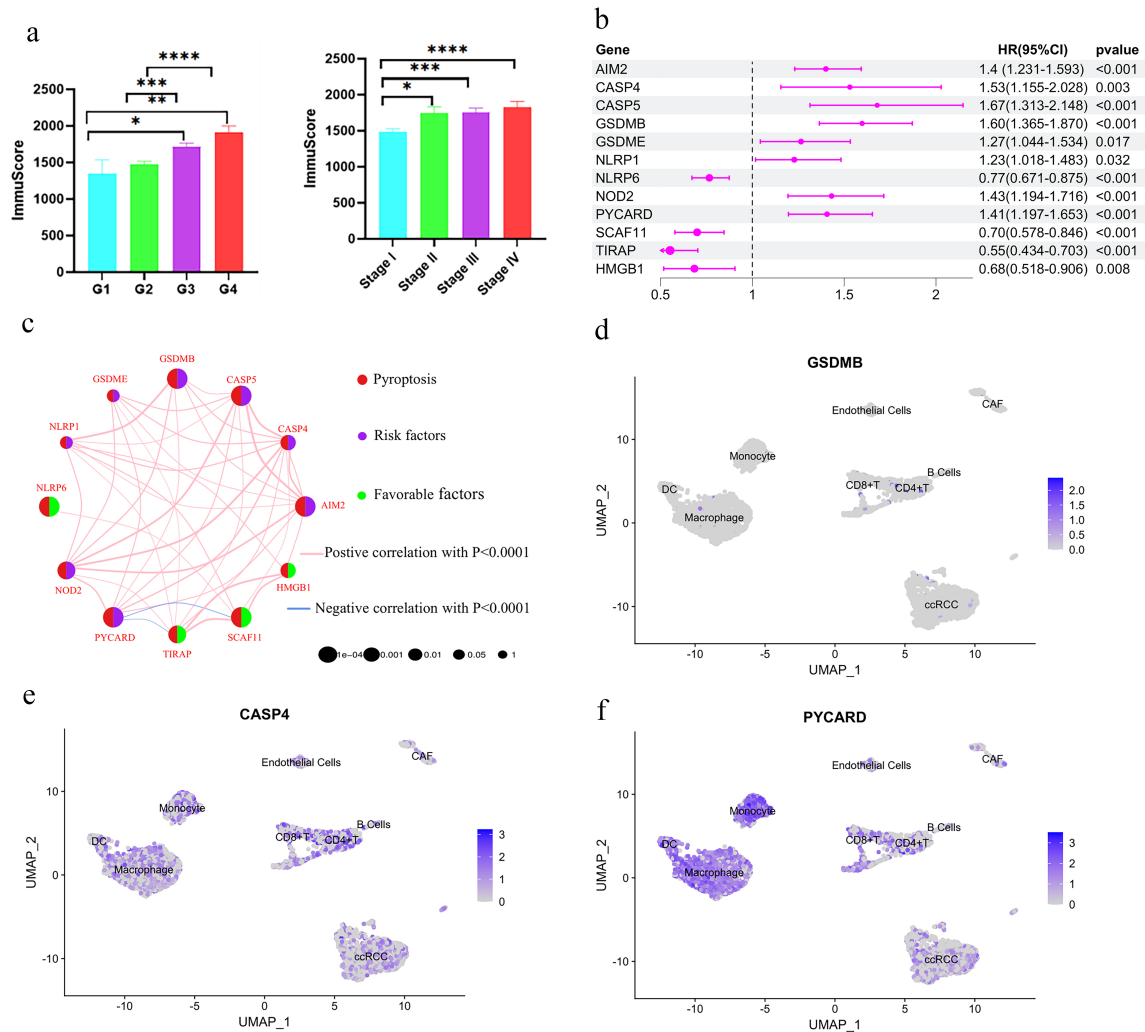


Fig. 1. Overview of pyroptosis-related genes in clear cell renal cell carcinoma (ccRCC). (a) Relationship between the Immune Score and tumor grade and stage ($*p < 0.05$; $**p < 0.01$; $***p < 0.001$; $****p < 0.0001$). (b) Forest plot presents pyroptosis-related genes associated with overall survival in ccRCC in The Cancer Genome Atlas (TCGA) database. (c) Interactions among pyroptosis-related genes (PRGs) in ccRCC. (The lines connecting PRGs indicate the interactions between them, while the width of the lines indicates the strength of the connection between them. Blue represents negative correlation and purple represents positive correlation, and the size of the point represents the strength of the p -value. Purple dots represent risk factors and green dots represent protective factors). (d–f) Expression of pyroptosis-related genes in the microenvironment of renal clear cell carcinoma based on single-cell RNA sequencing data.

vealed that Cluster 2 had more cancer-associated fibroblasts, while Cluster 1 had more endothelial cells. These results demonstrate that Cluster 1 tumors had increased angiogenesis, similar to the result from the TIMER database (Fig. 2e). Moreover, evaluation of the subsets at the protein level further support the clustering results in RPPA database (Supplementary Table 3). The AKT pS473, AMPKALPHA, c-KIT, EGFR pY1068, EGFR pY1173, MAPK pT202Y204, MEK1, SMAD1, SMAD4, CD31, VEGFR2, and STAT3 pY705 proteins were significantly expressed in Cluster 1 (Fig. 2f). These proteins participate in various carcinogenic processes and are also associated with angiogenesis. For example, CD31 is widely used as a

vascular marker to assess tumor angiogenesis [27,28], while VEGFR2 promotes angiogenesis by affecting the proliferation and migration of vascular endothelial cells [29]. Therefore, Cluster 1 was referred to as the “angiogenesis subtype” [30].

3.3 Cluster 2: Inflamed Phenotype

A recent study reported that high immune infiltration in ccRCC was associated with worse patient outcome [31]. The immune cells in the microenvironment between the two subtypes were evaluated based on CIBERSORT. Cluster 1 showed abundant infiltration of activated innate immune cells, including activated dendritic cells, M1

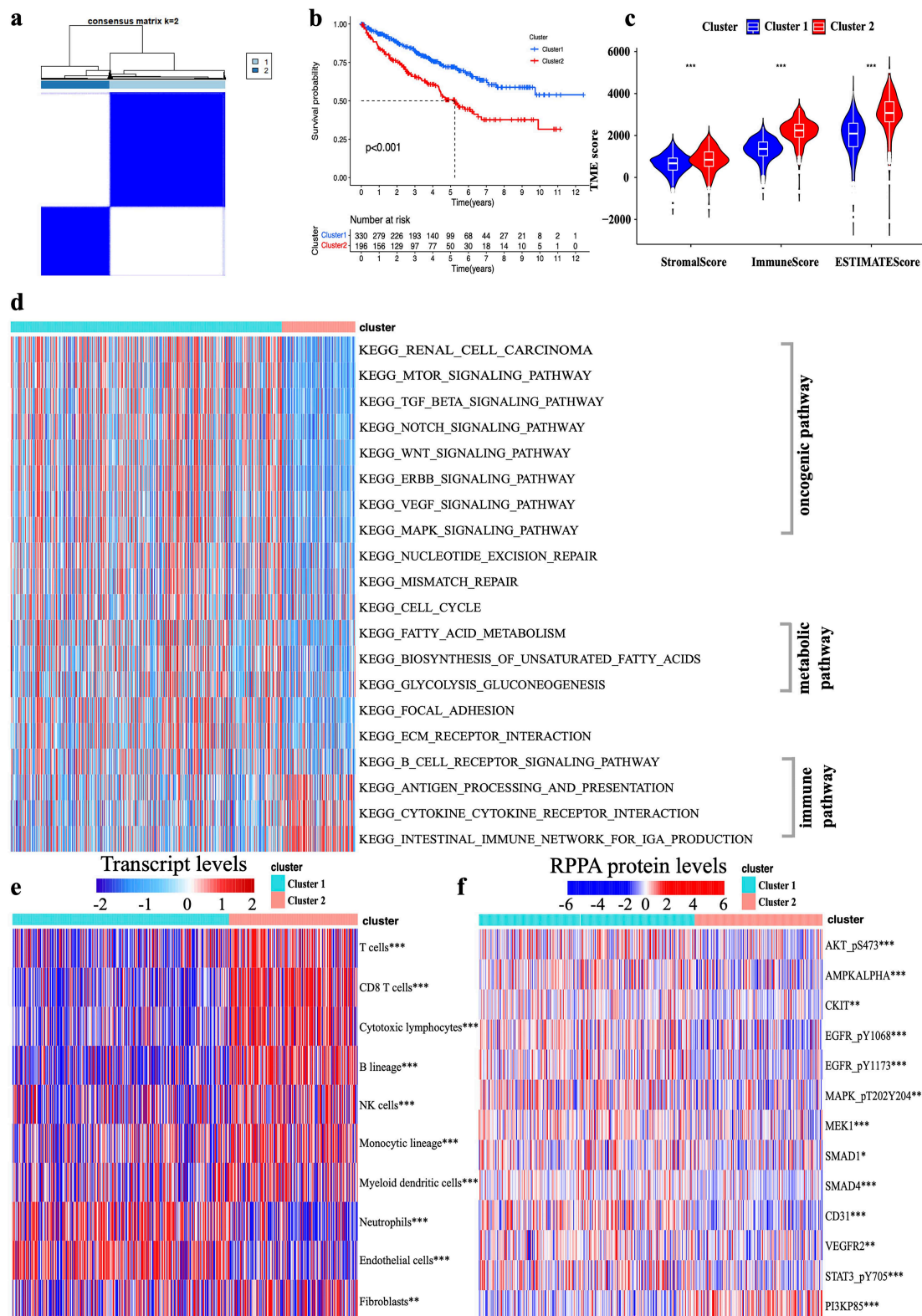


Fig. 2. Cluster 1 shows features of an angiogenesis phenotype. (a) 526 ccRCC patients were divided into two subtypes based on the consensus clustering matrix. (b) Analysis of overall survival in two subgroups. (c) Tumor microenvironment (TME) score in the two clusters ($***p < 0.001$). (d) Identification of common pathways in the two subtypes at the transcriptome level using gene set variation analysis (GSVA). (e) Comparison of the TME between the two subtypes at the transcriptional level based on the Tumor Immune Estimation Resource (TIMER) database ($**p < 0.01$; $***p < 0.001$). (f) Comparison of proteins associated with the angiogenic signalling pathway between the two subtypes based on the RPPA database ($*p < 0.05$; $**p < 0.01$; $***p < 0.001$).

macrophages, naïve B cells, resting NK cells, mast cells and resting T4 memory cells. Although Cluster 2 showed significant immune cell infiltration, this subgroup was enriched with regulatory T (Treg) cells and CD8⁺ T cells (Fig. 3b). KEGG pathway enrichment analysis revealed that DEGs were primarily enriched in immune-related pathways, with cytokines and cytokine-receptor interactions being the most significantly enriched. Consequently, we investigated chemokines, tumor necrosis factor and interleukin in the TME of the two subtypes. Cytokine expression was significantly different between the subtypes. IL-4, IL-10 and IL-6 are crucial for immunosuppression and can promote cancer metastasis [32]. IL-6 can also promote MDSC differentiation, thus promoting immunosuppression [33]. CXCL10, CCL4, CCL5, CCL8, CCL19 and CXCL13 have been associated with worse survival of ccRCC patients [34,35]. CCL5 recruits Treg cells into tumor masses [36]. Markers associated with T cell exhaustion, such as TIGIT, LAG3, LYN, and TOX, were significantly expressed in Cluster 2 (Fig. 3a). Although there were more infiltrating CD8⁺ T cells, the T cells in Cluster 2 were exhausted or non-functional, thus confirming our hypothesis. Single-cell RNA sequencing revealed heterogeneity among infiltrating CD8⁺ T cells in the ccRCC microenvironment, with most showing high expression levels for markers of exhaustion (Fig. 3c,d). Moreover, exhausted CD8⁺ T cells were associated with tumor stage [37]. Therefore, Cluster 2 was referred to as the “inflamed subtype” [38]. Anti-angiogenic therapy and immune checkpoint inhibitors, alone or in combination, can significantly improve the clinical prognosis of patients with advanced ccRCC. This is due to the high vascular density and the large number of immune cells infiltration in the microenvironment of ccRCC [39]. VEGF, VEGFR, EGF, EGFR, and KIT are targets for first-line anti-angiogenesis therapy. The expression of these targets and of immune checkpoints in the two subgroups was confirmed here (Fig. 3e). The results suggest the “angiogenesis subtype” may be more sensitive to targeted therapy, while the “inflamed subtype” may be more sensitive to immunotherapy.

3.4 Molecular Characteristics of the Two Subtypes and Differences in Treatment Response

The antitumor immune response requires a series of stepwise events termed the cancer immune cycle. Neoantigens produced by oncogenesis are first captured by dendritic cells (DCs) (step 1). The antigens captured by MHC I and MHC II molecules are then presented to T cells (step 2). Effector T cells are then primed and activated (step 3). Finally, the activated effector T cells move to the tumor bed (step 4) and subsequently infiltrate (step 5). As a result, they selectively recognize cancer cells through T-cell receptor (TCR) interactions (step 6) and kill the target cancer cell (step 7) [18]. Differences between the two subtypes were observed here for the cancer-immune cycle

(Fig. 4a). Cluster 2 had a higher score for step 7 due to more infiltration of CD8⁺ T cell. However, a high number of exhausted CD8⁺ T cells limits the recognition of cancer cells, and immune checkpoint blockade can re-awaken exhausted CD8⁺ T cells to elicit antitumor immunity [40]. The tumor mutation burden (TMB) is a biomarker of the immune checkpoint blockade response [41]. Commonly mutated genes in ccRCC were evaluated here in the two clusters. *BAP1* mutation was more frequent in Cluster 2, while *ATM* and *PBRM1* mutations were more frequent in Cluster 1 (Fig. 4b). The TMB was not statistically different between the two clusters (Supplementary Fig. 7). Tumors with *BAP1* mutation have been associated with considerably worse overall survival rates [42,43]. Furthermore, *BAP1*-mutant tumors are associated with mTORC1 activation [44]. The clinical features of the two clusters were investigated next. Tumors from Cluster 2 had higher grade, stage and immune score, thus explaining their worse prognosis (Fig. 4c). We further assessed genes that were previously related to specific biological processes [45]. Cluster 1 contains more oncogenic pathways such as epithelial-mesenchymal transition (EMT) and Wnt signaling, as well as the cell cycle and angiogenesis pathway (Fig. 4c). Cluster 2 was enriched in immune pathways, including CD8⁺ T effectors, immune checkpoint, and Pan-F-TBRS pathways. Personalized treatment for ccRCC could therefore be offered based on the characteristics of significant vascular infiltration in Cluster 1, and of immunosuppression in Cluster 2. Anti-angiogenic drugs that target VEGF signalling pathways, including sorafenib and sunitinib, have been widely used to treat advanced carcinomas [46,47]. In accordance with our conjecture, the Cluster 1 subgroup in the E-MTAB-3267 cohort showed a higher objective response rate to sunitinib than Cluster 2 (Fig. 4d). Based on the same genes, tumor samples in the PD-1 inhibitor-treated cohorts E-MTAB-3218 and CheckMate-010 were divided into two distinct subgroups, thus demonstrating the robustness of our cluster analysis (Fig. 4e,f). As predicted, Patients in cluster 2 had a higher reactivity to nivolumab than Cluster 1 patients.

3.5 Construction and Validation of a Prognostic Signature

A prognostic signature was developed to predict prognosis and the response to immune checkpoint blockade therapy. Univariate Cox regression analysis was performed using the MCC function to identify the top 30 central genes in the two subgroups associated with OS, followed by LASSO penalty Cox regression analysis of the significant variables ($p < 0.05$). A 9-gene signature was then constructed based on the optimum λ value. The risk score for each patient was calculated using the following formula: $(0.184 \times \text{HJURP exp}) + (0.329 \times \text{NUF2 exp}) + (-0.203 \times \text{KIF15 exp}) + (-0.390 \times \text{MELK exp}) + (-0.101 \times \text{TPX2 exp}) + (0.250 \times \text{PLK1 exp}) + (0.561 \times \text{CDCA3 exp}) + (0.050 \times \text{CTLA4 exp}) + (0.050 \times \text{FOXP3 exp})$. Patients in the TCGA dataset

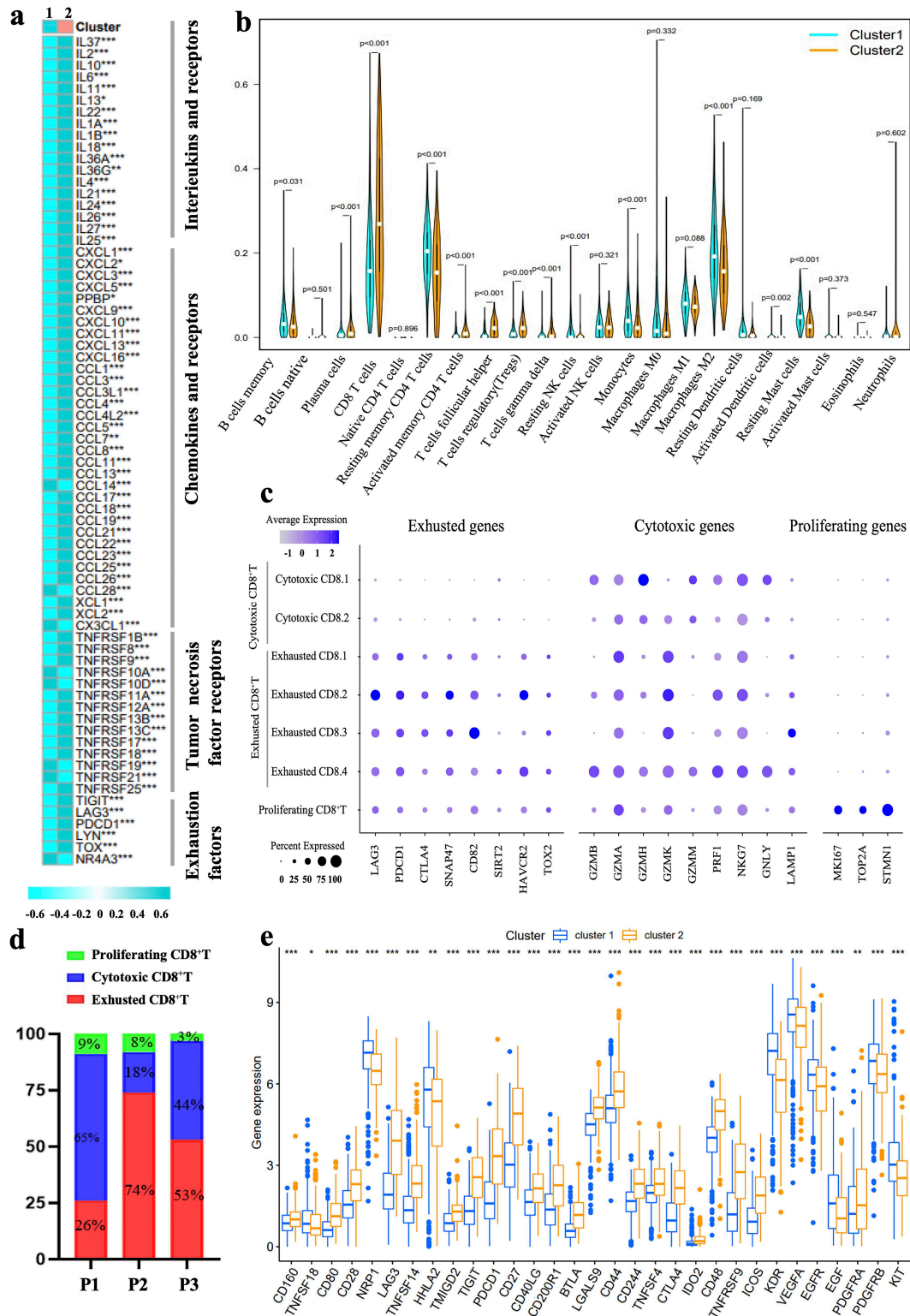


Fig. 3. Cluster 2 shows an inflamed phenotype. (a) The thermogram shows different expression for chemokines, interleukins, tumor necrosis factor and T cell exhaustion factors between Clusters 1 and 2 at the transcriptome level ($*p < 0.05$; $**p < 0.01$, $***p < 0.001$). (b) The abundance of infiltrating immune cells in the tumor microenvironment was analyzed separately for the two pyroptosis-related clusters using CIBERSORTx. (c) Characteristics of CD8⁺ T cells in the tumor microenvironment of ccRCC. (d) Percentage of exhausted CD8⁺ T cells in the TME (P1 represents the first patient, P2 means the second patient, and P3 means the third patient). (e) Expression levels of angiogenic genes and immune checkpoint genes at the transcriptome level between the two subtypes ($*p < 0.05$; $**p < 0.01$; $***p < 0.001$).

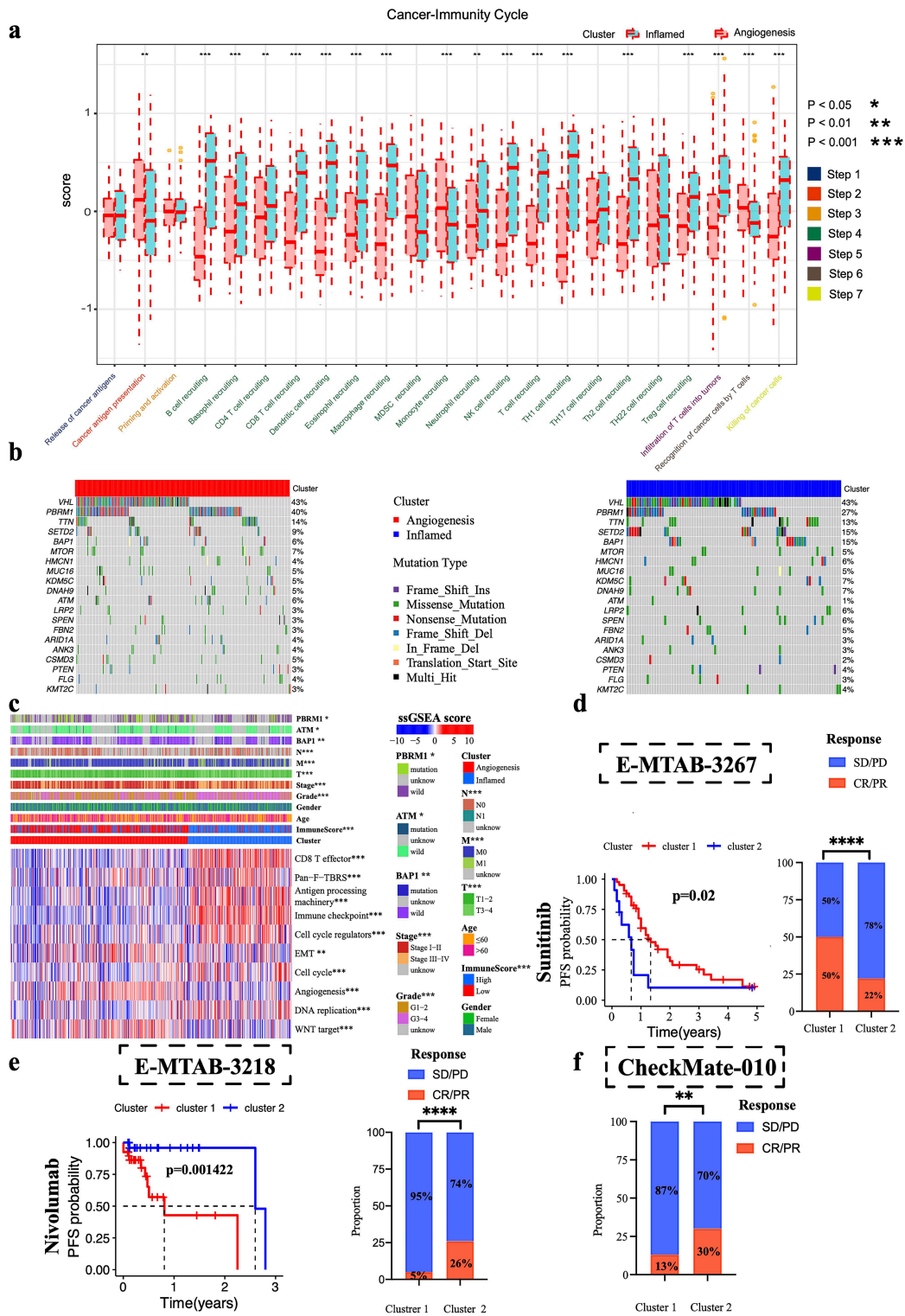


Fig. 4. Comprehensive analysis of clinical and mutational features of the two clusters, as well as their response to treatment. (a) Cancer immune cycle analysis in the two clusters. (b) The top 20 mutations found in the two subtypes of ccRCC. (c) The clinical features, mutation and functional characteristics of the subtypes were comprehensively analyzed (* $p < 0.05$; ** $p < 0.01$; *** $p < 0.001$). (d) Response of the two subtypes to sunitinib therapy (*** $p < 0.0001$). (e) The response to nivolumab treatment was assessed between the two subtypes using progression-free survival (CR means complete response; PR means partial response; SD means stable disease; PD means progressive disease) (*** $p < 0.0001$). (f) Response of the two subtypes to nivolumab therapy in CheckMate-010 cohort (** $p < 0.01$).

were then divided into high- and low-risk groups according to the median score. Survival analysis revealed the low-risk group had a significantly better clinical outcome than the high-risk group (Fig. 5a; $p < 0.01$). Using the same algorithm, risk scores were calculated for ccRCC patients classified as low- and high-risk subgroups in the E-MTAB-1980 dataset to further validate the prognostic signature. Kaplan-Meier survival curves showed the OS results for ccRCC patient subgroups was consistent with those from the TCGA dataset (Fig. 5c; $p < 0.001$). To investigate whether this signature could also predict responsiveness to PD-1 therapy, risk scores were calculated using the same algorithm in the CheckMate-025 and CheckMate-010 datasets for metastatic ccRCC patients previously treated with VEGF-directed therapy. The signature predicted both progression-free survival (PFS) and OS of metastatic ccRCC patients treated with nivolumab. The low-risk group showed better response to nivolumab treatment than the high-risk group (Fig. 5e,f). Moreover, in the IMvigor210 cohort the risk score also reflected objective response rates and PFS in urothelial carcinoma patients treated with the PD-L1 inhibitor atezolizumab (Supplementary Fig. 8). Univariate and multivariate Cox analyses were also used to evaluate whether the signature was an independent prognostic factor for ccRCC patients. Univariate analysis indicated the signature was strongly associated with OS in ccRCC patients from the TCGA dataset [hazard ratio (HR): 3.08 95% CI: 2.46–3.85, $p < 0.001$]. Multivariate analysis further showed the signature was an independent predictor of OS (HR: 2.10, 95% CI: 1.63–2.70, $p < 0.001$; Fig. 5g). The test dataset confirmed the signature was an independent predictor of OS for ccRCC patients in univariate (HR: 4.16, 95% CI: 2.46–7.03, $p < 0.001$) and multivariate (HR: 3.62, 95% CI: 1.89–6.95, $p < 0.001$) analyses (Fig. 5h). These results indicate the 9-gene signature may be useful for the clinical evaluation of prognosis. AUC analysis of cases in the TCGA database revealed the signature showed good accuracy, with values of 0.73, 0.72 and 0.75 at 1, 5 and 10 years of follow-up, respectively (Fig. 5b). The AUC values calculated from the E-MTAB-1980 dataset were 0.89, 0.82 and 0.75 at 1, 5 and 10 years, respectively (Fig. 5d).

3.6 GSDMB Expression is Associated with ccRCC Progression and Poor Prognosis

The PRGs with prognostic significance were associated with immune cell infiltration, immune checkpoints (Fig. 6a), and activation of the epithelial-mesenchymal transition (EMT) (Fig. 6b). Multivariate cox regression analysis showed that GSDMB was the most significant prognostic factor for ccRCC compared with other pyroptosis-related genes (Fig. 6c). Moreover, GSDMB was overexpressed in ccRCC tissue in GSE40435 and GSE53757 from the GEO dataset (Supplementary Fig. 9). Kaplan-Meier analysis showed that GSDMB overexpression was associated with poor OS of ccRCC patients (Supplementary Fig.

10). The TCGA database showed that GSDMB overexpression was significantly correlated to the stage and grade of ccRCC (Fig. 6d–f). qPCR showed that GSDMB expression at the transcription level was associated with ccRCC grade (Supplementary Fig. 11). Differential expression of GSDMD at the protein level was found between ccRCC cells and normal kidney cells, confirming previous findings (Fig. 6g,h). Furthermore, IHC revealed that GSDMB expression was related to ccRCC grade (Fig. 6i,j). Therefore, the above results indicate that GSDMB may promote the occurrence and development of renal clear cell carcinoma, although the precise mechanisms remain to be determined.

4. Discussion

ccRCC is an immunogenic cancer with a substantial proportion of cytolytic, tumor-infiltrating lymphocytes (TILs), thus making it a candidate tumor for immunotherapy. In the present study, the role of pyroptosis in ccRCC was further explored with the aim of achieving more individualized patient therapy treatment. Tumor samples were first divided into two subtypes according to their expression of pyroptosis-associated genes with prognostic significance. The two subtypes showed significantly different OS amongst ccRCC patients and were thus comprehensively analyzed at the genomic, transcriptomic and protein levels to explore differences. *BAP1* mutation was more frequent in Cluster 2, while *ATM* and *PBRM1* mutations were more frequent in Cluster 1. Patients with *BAP1* mutations had higher tumor grade and shorter overall survival. Moreover, recent studies have shown that alterations to *PBRM1* can predict the response to immunotherapy in patients with renal cell carcinoma [48,49]. GSVA analysis showed Cluster 1 was enriched for carcinogenic activation pathways, various metabolic pathways, and cell cycle pathways. Cluster 2 was enriched for immune pathways. Evaluation of stromal components and immune cells in the TME revealed that Cluster 2 had more infiltrating immune cells, cancer-associated fibroblasts and stromal cells. Further analysis of the stromal cells showed that Cluster 1 had more endothelial cells. Cluster 1 was also associated with canonical oncogenic pathways, especially angiogenesis, and was therefore named the angiogenic phenotype. In contrast, Cluster 2 was named the inflamed phenotype because it showed more infiltration with $CD8^+$ T cells and Treg cells, and more immunosuppressive and T-cell exhaustion factors in the TME. Treg cells are the key suppressive cells among the tumor-infiltrating lymphocytes (TIL) and can indicate poor prognosis [50]. Unlike other tumor types, $CD8^+$ T cells are associated with poor prognosis in ccRCC, Previous studies have shown that extensive infiltration with $CD8^+$ T cells is associated with poor prognosis in patients with primary and metastatic ccRCC [51]. This may be one of the reasons for the poor prognosis observed here for cluster 2 Tumors from Cluster 2 had higher grade and stage than those from Cluster 1, which may ex-

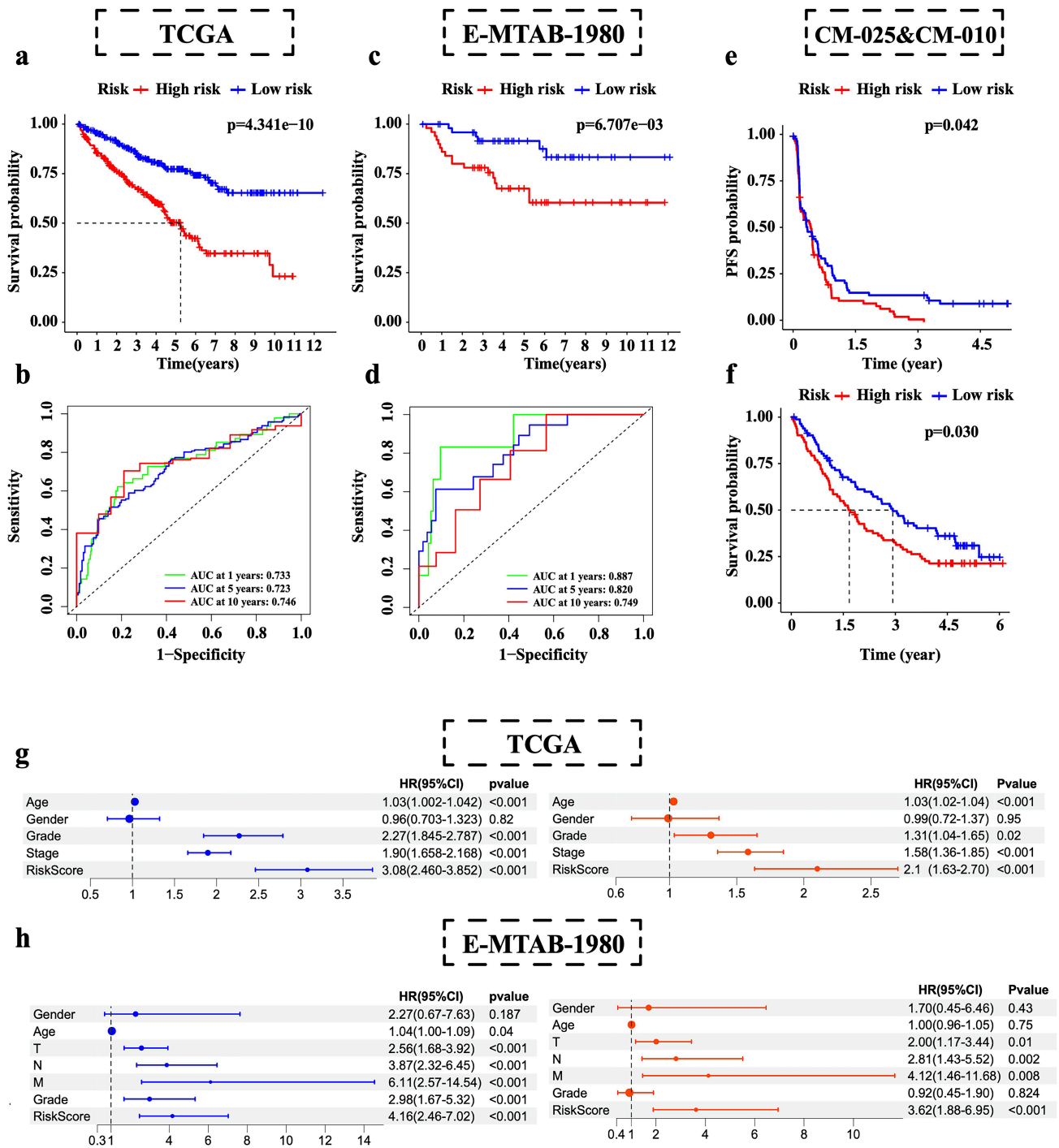


Fig. 5. Construction and validation of a subtype-based prognostic signature. (a) Survival analysis of high- and low-risk groups in patients from the TCGA database. (b) Receiver operating characteristic (ROC) curves demonstrated the accuracy of the risk score in the TCGA database. (c) Overall survival (OS) analysis of the high- and low-risk groups in patients from the E-MTAB-1980 cohort. (d) ROC curves demonstrated the accuracy of the risk score in the E-MTAB-1980 dataset. (e) Progression-free survival (PFS) in the high- and low-risk groups of patients from the CheckMate-025 and CheckMate-010 cohorts. (f) OS in the high- and low-risk groups of patients from the CheckMate-025 and CheckMate-010 cohorts. (g) Univariate (left) and multivariate (right) analysis of the training set from the TCGA cohort. (h) Univariate analysis (left) and multivariate (right) analysis of the test set from the E-MTAB-1980 cohort.

plain why Cluster 2 patients had significantly worse prognosis than those from Cluster 1. Differential expression of angiogenesis-related genes and of immune checkpoints fur-

ther confirmed the cluster phenotypes. Moreover, evaluation of specific steps in the tumor immune cycle revealed the T cells in Cluster 2 had low ability to recognize tu-

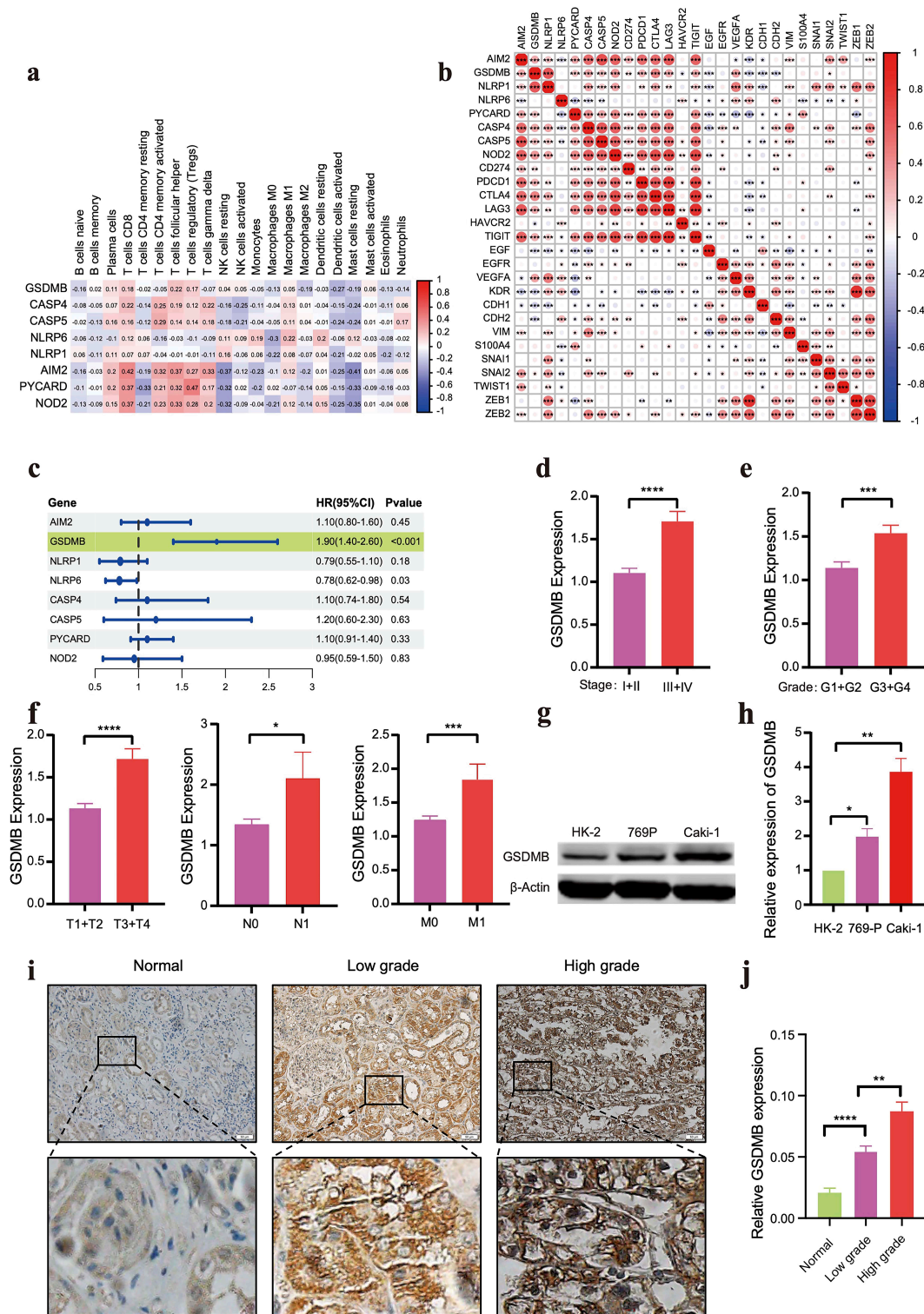


Fig. 6. Comprehensive analysis of clinical features associated with the two clusters. (a) Relationship between 8 prognostic genes and infiltrating immune cells in the microenvironment. (b) Relationship between expression of the 8 prognostic genes, angiogenesis-related genes, and epithelial-mesenchymal transition (EMT)-related genes. (c) Multivariate cox regression analysis of overall survival was performed for 8 pyroptosis-related genes. (d–f) Relationship between GSDMB and clinical features of clear cell renal cell carcinoma ($*p < 0.05$; $***p < 0.001$; $****p < 0.0001$). (g,h) Relative level of GSDMB protein expression in the HK-2, Caki-1 and 769P cell lines ($*p < 0.05$; $**p < 0.01$). (i) Representative IHC staining for GSDMB in normal, low and high grade ccRCC. (j) GSDMB expression level in normal ($n = 15$), low grade ($n = 15$) and high grade ($n = 5$) ccRCC tissues ($*p < 0.01$; $****p < 0.0001$).

mor cells. Thirty hub genes were used to build a model for predicting the sensitivity to anti-PDL1 therapy. A 9-gene prognostic signature (*HJURP*, *NUF2*, *MELK*, *TPX2*, *PLK1*, *CDCA3*, *CTLA4*, *FOXP3*, *KIF15*) was identified using univariate and LASSO regression analyses. These genes have been implicated in the progression and treatment resistance of various cancer types [52,53]. The signature could predict the outcome of ccRCC patients in both the TCGA and E-MTAB-1980 datasets. Immunotherapy drugs such as nivolumab prolong the survival of patients with metastatic ccRCC [54,55], although the response rates are lower than for other solid tumors. Reliable and robust biomarkers for the response to immunotherapy are therefore required. Of note, our 9-gene signature showed predictive value (Progression-free survival and Overall survival) for anti-PD1 therapy, and suggested that low-risk patients may derive benefit from immune checkpoint blockade therapy. IHC showed that *GSDMB* was differentially expressed between normal renal tissue and low- and high-grade ccRCC. Similarly, *GSDMB* was differentially expressed between HK-2 normal and Caki-1 and 769-P tumor cell lines based on Western blot. The anti-cancer role of tumor cell pyrolysis has recently attracted considerable interest. For instance, *GSDMB* was also promotes the proliferation and invasion by activating the STAT3 signaling pathway in bladder cancer [56]. However, a limitation of the present study is that data on several important clinical variables (e.g., surgery, neoadjuvant chemotherapy, chemoradiotherapy) was unavailable for most datasets. This may have affected the apparent prognostic value found here for the immune response and pyroptosis state in ccRCC. Therefore, additional research on the mechanism of pyroptosis may allow further insight into the role of pyroptosis in ccRCC and provide a theoretical basis for personalized treatment.

5. Conclusions

In summary, two subgroups of ccRCC patients were identified based on the expression of pyroptosis-related genes. A robust prognostic signature was also developed using the expression of 9 core genes. The expression of *GSDMB* was associated with ccRCC progression. Further studies are needed to confirm the specific role of pyroptosis-related genes in ccRCC and to identify the associated regulatory mechanisms.

Abbreviations

RCC, Renal cell carcinoma; ccRCC, clear cell renal cell carcinoma; GSVA, gene set variation analysis; TCGA, The Cancer Genome Atlas; GEO, Gene Expression Omnibus; PRGs, pyroptosis-related genes; TMB, tumor mutation burden; MCC, Maximal Click Centrality; LASSO, least absolute shrinkage, and selection operator; EMT, epithelial-mesenchymal transition.

Availability of Data and Materials

All datasets can be downloaded from The Cancer Genome Atlas (TCGA) (<https://portal.gdc.cancer.gov/>) databases, Gene Expression Omnibus (GEO) (<https://www.ncbi.nlm.nih.gov/geo/>), ArrayExpress database (<https://www.ebi.ac.uk/arrayexpress/>), CheckMate 025 was from (CM-025; NCT01668784) and CheckMate-010 was from (CM-010; NCT01354431). Details are listed in the Materials and Methods section.

Author Contributions

ZW, LW and WX conceived and designed the study. JM, ZK and GY contributed experimental design, data collection, data analysis and data presentation. XW, MS and YW provided expertise in design of study and interpretation of data. GL, SB, FZ and ML performed and analyzed the Western blotting and Immunohistochemistry, JM was responsible for the study design, manuscript writing, and the whole process of manuscript submission. All authors contributed to editorial changes in the manuscript. All authors read and approved the final manuscript. All authors have participated sufficiently in the work and agreed to be accountable for all aspects of the work.

Ethics Approval and Consent to Participate

The study was approved by the Ethics Committee of the Fourth Affiliated Hospital, Harbin Medical University (approval ID: 2023-YXLLSC-08). Informed consent was obtained and signed by patients for all tissues.

Acknowledgment

We appreciate the platforms and datasets from TCGA, GEO, and STRING.

Funding

National Natural Science Foundation of China (82172000 and 81971135 and U20A20385); Natural Science Foundation of Gansu Province (21JR11RA172).

Conflict of Interest

The authors declare no conflict of interest.

Supplementary Material

Supplementary material associated with this article can be found, in the online version, at <https://doi.org/10.31083/j.fbl2812334>.

References

- [1] Sung H, Ferlay J, Siegel RL, Laversanne M, Soerjomataram I, Jemal A, *et al.* Global Cancer Statistics 2020: GLOBOCAN Estimates of Incidence and Mortality Worldwide for 36 Cancers in 185 Countries. *CA: A Cancer Journal for Clinicians*. 2021; 71: 209–249.
- [2] Moch H, Cubilla AL, Humphrey PA, Reuter VE, Ulbright TM.

The 2016 WHO Classification of Tumours of the Urinary System and Male Genital Organs-Part A: Renal, Penile, and Testicular Tumours. *European Urology*. 2016; 70: 93–105.

- [3] Cohen HT, McGovern FJ. Renal-cell carcinoma. *The New England Journal of Medicine*. 2005; 353: 2477–2490.
- [4] Shuch B, Amin A, Armstrong AJ, Eble JN, Ficarra V, Lopez-Beltran A, *et al.* Understanding pathologic variants of renal cell carcinoma: distilling therapeutic opportunities from biologic complexity. *European Urology*. 2015; 67: 85–97.
- [5] Heng DYC, Xie W, Regan MM, Warren MA, Golshayan AR, Sahi C, *et al.* Prognostic factors for overall survival in patients with metastatic renal cell carcinoma treated with vascular endothelial growth factor-targeted agents: results from a large, multicenter study. *Journal of Clinical Oncology: Official Journal of the American Society of Clinical Oncology*. 2009; 27: 5794–5799.
- [6] di Martino S, De Luca G, Grassi L, Federici G, Alfonsi R, Signore M, *et al.* Renal cancer: new models and approach for personalizing therapy. *Journal of Experimental & Clinical Cancer Research: CR*. 2018; 37: 217.
- [7] Glynne-Jones R, Wyrwicz L, Tiret E, Brown G, Rödel C, Cervantes A, *et al.* Rectal cancer: ESMO Clinical Practice Guidelines for diagnosis, treatment and follow-up. *Annals of Oncology: Official Journal of the European Society for Medical Oncology*. 2017; 28: iv22–iv40.
- [8] Sharma BR, Kanneganti TD. Inflammasome signaling in colorectal cancer. *Translational Research: the Journal of Laboratory and Clinical Medicine*. 2023; 252: 45–52.
- [9] Xia X, Wang X, Cheng Z, Qin W, Lei L, Jiang J, *et al.* The role of pyroptosis in cancer: pro-cancer or pro-“host”? *Cell Death & Disease*. 2019; 10: 650.
- [10] Gao J, Qiu X, Xi G, Liu H, Zhang F, Lv T, *et al.* Downregulation of GSDMD attenuates tumor proliferation via the intrinsic mitochondrial apoptotic pathway and inhibition of EGFR/Akt signaling and predicts a good prognosis in non small cell lung cancer. *Oncology Reports*. 2018; 40: 1971–1984.
- [11] Wilkerson MD, Hayes DN. ConsensusClusterPlus: a class discovery tool with confidence assessments and item tracking. *Bioinformatics (Oxford, England)*. 2010; 26: 1572–1573.
- [12] Hänzelmann S, Castelo R, Guinney J. GSVA: gene set variation analysis for microarray and RNA-seq data. *BMC Bioinformatics*. 2013; 14: 7.
- [13] Ritchie ME, Phipson B, Wu D, Hu Y, Law CW, Shi W, *et al.* limma powers differential expression analyses for RNA-sequencing and microarray studies. *Nucleic Acids Research*. 2015; 43: e47.
- [14] Becht E, Giraldo NA, Lacroix L, Buttard B, Elarouci N, Petitprez F, *et al.* Estimating the population abundance of tissue-infiltrating immune and stromal cell populations using gene expression. *Genome Biology*. 2016; 17: 218.
- [15] Newman AM, Liu CL, Green MR, Gentles AJ, Feng W, Xu Y, *et al.* Robust enumeration of cell subsets from tissue expression profiles. *Nature Methods*. 2015; 12: 453–457.
- [16] Yoshihara K, Shahmoradgoli M, Martínez E, Vegesna R, Kim H, Torres-García W, *et al.* Inferring tumour purity and stromal and immune cell admixture from expression data. *Nature Communications*. 2013; 4: 2612.
- [17] Li T, Fu J, Zeng Z, Cohen D, Li J, Chen Q, *et al.* TIMER2.0 for analysis of tumor-infiltrating immune cells. *Nucleic Acids Research*. 2020; 48: W509–W514.
- [18] Chen DS, Mellman I. Oncology meets immunology: the cancer-immunity cycle. *Immunity*. 2013; 39: 1–10.
- [19] Xu L, Deng C, Pang B, Zhang X, Liu W, Liao G, *et al.* TIP: A Web Server for Resolving Tumor Immunophenotype Profiling. *Cancer Research*. 2018; 78: 6575–6580.
- [20] Lossos IS, Czerwinski DK, Alizadeh AA, Wechser MA, Tibshirani R, Botstein D, *et al.* Prediction of survival in diffuse large-B-cell lymphoma based on the expression of six genes. *The New England Journal of Medicine*. 2004; 350: 1828–1837.
- [21] Lun ATL, Bach K, Marioni JC. Pooling across cells to normalize single-cell RNA sequencing data with many zero counts. *Genome Biology*. 2016; 17: 75.
- [22] McCarthy DJ, Campbell KR, Lun ATL, Wills QF. Scater: pre-processing, quality control, normalization and visualization of single-cell RNA-seq data in R. *Bioinformatics (Oxford, England)*. 2017; 33: 1179–1186.
- [23] Haghverdi L, Lun ATL, Morgan MD, Marioni JC. Batch effects in single-cell RNA-sequencing data are corrected by matching mutual nearest neighbors. *Nature Biotechnology*. 2018; 36: 421–427.
- [24] Thompson RH, Dong H, Lohse CM, Leibovich BC, Blute ML, Chevillet JC, *et al.* PD-1 is expressed by tumor-infiltrating immune cells and is associated with poor outcome for patients with renal cell carcinoma. *Clinical Cancer Research: an Official Journal of the American Association for Cancer Research*. 2007; 13: 1757–1761.
- [25] Xu WH, Xu Y, Wang J, Wan FN, Wang HK, Cao DL, *et al.* Prognostic value and immune infiltration of novel signatures in clear cell renal cell carcinoma microenvironment. *Aging*. 2019; 11: 6999–7020.
- [26] Zhang Z, Zhang Y, Lieberman J. Lighting a Fire: Can We Harness Pyroptosis to Ignite Antitumor Immunity? *Cancer Immunology Research*. 2021; 9: 2–7.
- [27] Goel HL, Pursell B, Chang C, Shaw LM, Mao J, Simin K, *et al.* GLI1 regulates a novel neuropilin-2/ $\alpha 6\beta 1$ integrin based autocrine pathway that contributes to breast cancer initiation. *EMBO Molecular Medicine*. 2013; 5: 488–508.
- [28] Lu D, Wang J, Li Y, Zhang Y, Yu L, Xu T, *et al.* Tumor Noninvasive and Target Embolization Therapy Platform by Intravenous Injection Based on Acidic Microenvironment-Responsive Hyperbranched Poly(amino acid)s. *ACS Central Science*. 2020; 6: 1977–1986.
- [29] Shaik S, Nucera C, Inuzuka H, Gao D, Garnaas M, Frechette G, *et al.* SCF(β -TRCP) suppresses angiogenesis and thyroid cancer cell migration by promoting ubiquitination and destruction of VEGF receptor 2. *The Journal of Experimental Medicine*. 2012; 209: 1289–1307.
- [30] Motzer RJ, Banchereau R, Hamidi H, Powles T, McDermott D, Atkins MB, *et al.* Molecular Subsets in Renal Cancer Determine Outcome to Checkpoint and Angiogenesis Blockade. *Cancer Cell*. 2020; 38: 803–817.e4.
- [31] Iglesia MD, Parker JS, Hoadley KA, Serody JS, Perou CM, Vincent BG. Genomic Analysis of Immune Cell Infiltrates Across 11 Tumor Types. *Journal of the National Cancer Institute*. 2016; 108: djw144.
- [32] Miao L, Li J, Liu Q, Feng R, Das M, Lin CM, *et al.* Transient and Local Expression of Chemokine and Immune Checkpoint Traps To Treat Pancreatic Cancer. *ACS Nano*. 2017; 11: 8690–8706.
- [33] Mace TA, Shakya R, Pitarresi JR, Swanson B, McQuinn CW, Loftus S, *et al.* IL-6 and PD-L1 antibody blockade combination therapy reduces tumour progression in murine models of pancreatic cancer. *Gut*. 2018; 67: 320–332.
- [34] Qu G, Wang H, Yan H, Liu G, Wu M. Identification of CXCL10 as a Prognostic Biomarker for Clear Cell Renal Cell Carcinoma. *Frontiers in Oncology*. 2022; 12: 857619.
- [35] Xu W, Ma C, Liu W, Anwaier A, Tian X, Shi G, *et al.* Prognostic value, DNA variation and immunologic features of a tertiary lymphoid structure-related chemokine signature in clear cell renal cell carcinoma. *Cancer Immunology, Immunotherapy: CII*. 2022; 71: 1923–1935.
- [36] Wang X, Lang M, Zhao T, Feng X, Zheng C, Huang C, *et al.* Cancer-FOXP3 directly activated CCL5 to recruit FOXP3⁺Treg

- cells in pancreatic ductal adenocarcinoma. *Oncogene*. 2017; 36: 3048–3058.
- [37] Braun DA, Street K, Burke KP, Cookmeyer DL, Denize T, Pedersen CB, *et al.* Progressive immune dysfunction with advancing disease stage in renal cell carcinoma. *Cancer Cell*. 2021; 39: 632–648.e8.
- [38] Zhang Z, Fan W, Deng Q, Tang S, Wang P, Xu P, *et al.* The prognostic and diagnostic value of circulating tumor cells in bladder cancer and upper tract urothelial carcinoma: a meta-analysis of 30 published studies. *Oncotarget*. 2017; 8: 59527–59538.
- [39] Choueiri TK, Motzer RJ. Systemic Therapy for Metastatic Renal-Cell Carcinoma. *The New England Journal of Medicine*. 2017; 376: 354–366.
- [40] Wei SC, Levine JH, Cogdill AP, Zhao Y, Anang NAAS, Andrews MC, *et al.* Distinct Cellular Mechanisms Underlie Anti-CTLA-4 and Anti-PD-1 Checkpoint Blockade. *Cell*. 2017; 170: 1120–1133.e17.
- [41] Offin M, Rizvi H, Tenet M, Ni A, Sanchez-Vega F, Li BT, *et al.* Tumor Mutation Burden and Efficacy of EGFR-Tyrosine Kinase Inhibitors in Patients with *EGFR*-Mutant Lung Cancers. *Clinical Cancer Research: an Official Journal of the American Association for Cancer Research*. 2019; 25: 1063–1069.
- [42] Kapur P, Peña-Llopis S, Christie A, Zhrebker L, Pavia-Jiménez A, Rathmell WK, *et al.* Effects on survival of BAP1 and PBRM1 mutations in sporadic clear-cell renal-cell carcinoma: a retrospective analysis with independent validation. *The Lancet. Oncology*. 2013; 14: 159–167.
- [43] Peña-Llopis S, Vega-Rubín-de-Celis S, Liao A, Leng N, Pavia-Jiménez A, Wang S, *et al.* BAP1 loss defines a new class of renal cell carcinoma. *Nature Genetics*. 2012; 44: 751–759.
- [44] Brugarolas J. Molecular genetics of clear-cell renal cell carcinoma. *Journal of Clinical Oncology: Official Journal of the American Society of Clinical Oncology*. 2014; 32: 1968–1976.
- [45] Mariathasan S, Turley SJ, Nickles D, Castiglioni A, Yuen K, Wang Y, *et al.* TGF β attenuates tumour response to PD-L1 blockade by contributing to exclusion of T cells. *Nature*. 2018; 554: 544–548.
- [46] Chen G, Xu X, Zhang L, Fu Y, Wang M, Gu H, *et al.* Blocking autocrine VEGF signaling by sunitinib, an anti-cancer drug, promotes embryonic stem cell self-renewal and somatic cell reprogramming. *Cell Research*. 2014; 24: 1121–1136.
- [47] Heng DY, Choueiri TK, Rini BI, Lee J, Yuasa T, Pal SK, *et al.* Outcomes of patients with metastatic renal cell carcinoma that do not meet eligibility criteria for clinical trials. *Annals of Oncology: Official Journal of the European Society for Medical Oncology*. 2014; 25: 149–154.
- [48] Farley MN, Schmidt LS, Mester JL, Pena-Llopis S, Pavia-Jimenez A, Christie A, *et al.* A novel germline mutation in BAP1 predisposes to familial clear-cell renal cell carcinoma. *Molecular Cancer Research: MCR*. 2013; 11: 1061–1071.
- [49] Bihl S, Ohashi R, Moore AL, Rüschoff JH, Beisel C, Hermanns T, *et al.* Expression and Mutation Patterns of PBRM1, BAP1 and SETD2 Mirror Specific Evolutionary Subtypes in Clear Cell Renal Cell Carcinoma. *Neoplasia (New York, N.Y.)*. 2019; 21: 247–256.
- [50] Liu Z, McMichael EL, Shayan G, Li J, Chen K, Srivastava R, *et al.* Novel Effector Phenotype of Tim-3⁺ Regulatory T Cells Leads to Enhanced Suppressive Function in Head and Neck Cancer Patients. *Clinical Cancer Research: an Official Journal of the American Association for Cancer Research*. 2018; 24: 4529–4538.
- [51] Giraldo NA, Becht E, Pagès F, Skliris G, Verkarre V, Vano Y, *et al.* Orchestration and Prognostic Significance of Immune Checkpoints in the Microenvironment of Primary and Metastatic Renal Cell Cancer. *Clinical Cancer Research: an Official Journal of the American Association for Cancer Research*. 2015; 21: 3031–3040.
- [52] Liu Y, Cheng G, Huang Z, Bao L, Liu J, Wang C, *et al.* Long non-coding RNA SNHG12 promotes tumour progression and sunitinib resistance by upregulating CDCA3 in renal cell carcinoma. *Cell Death & Disease*. 2020; 11: 515.
- [53] Shin SB, Woo SU, Yim H. Cotargeting Plk1 and androgen receptor enhances the therapeutic sensitivity of paclitaxel-resistant prostate cancer. *Therapeutic Advances in Medical Oncology*. 2019; 11: 1758835919846375.
- [54] Miao D, Margolis CA, Gao W, Voss MH, Li W, Martini DJ, *et al.* Genomic correlates of response to immune checkpoint therapies in clear cell renal cell carcinoma. *Science (New York, N.Y.)*. 2018; 359: 801–806.
- [55] Motzer RJ, Escudier B, McDermott DF, George S, Hammers HJ, Srinivas S, *et al.* Nivolumab versus Everolimus in Advanced Renal-Cell Carcinoma. *The New England Journal of Medicine*. 2015; 373: 1803–1813.
- [56] He H, Yi L, Zhang B, Yan B, Xiao M, Ren J, *et al.* USP24-GSDMB complex promotes bladder cancer proliferation via activation of the STAT3 pathway. *International Journal of Biological Sciences*. 2021; 17: 2417–2429.